β2-Adrenergic receptor agonist ameliorates phenotypes and corrects microRNA-mediated IGF1 deficits in a mouse model of Rett syndrome

Nikolaos Mellios[a,1], Jonathan Woodson[a], Rodrigo I. Garcia[a], Benjamin Crawford[a], Jitendra Sharma[a], Steven D. Sheridan[a,b], Stephen J. Haggarty[b], and Mriganka Sur[a,1]

[a]Department of Brain and Cognitive Sciences, Picower Institute for Learning and Memory, Massachusetts Institute of Technology, Cambridge, MA 02139; and [b]Center for Human Genetic Research, Department of Neurology, Massachusetts General Hospital, Harvard Medical School, Boston, MA 02114

Rett syndrome is a severe childhood onset neurodevelopmental disorder caused by mutations in methyl-CpG–binding protein 2 (*MECP2*), with known disturbances in catecholamine synthesis. Here, we show that treatment with the β2-adrenergic receptor agonist clenbuterol increases survival, rescues abnormalities in respiratory function and social recognition, and improves motor coordination in young male *Mecp2*-null (*Mecp2$^{-/y}$*) mice. Importantly, we demonstrate that short-term treatment with clenbuterol in older symptomatic female heterozygous (*Mecp2$^{-/+}$*) mice rescues respiratory, cognitive, and motor coordination deficits, and induces an anxiolytic effect. In addition, we reveal abnormalities in a microRNA-mediated pathway, downstream of brain-derived neurotrophic factor that affects insulin-like growth factor 1 (IGF1) expression in *Mecp2$^{-/y}$* mice, and show that treatment with clenbuterol restores the observed molecular alterations. Finally, cotreatment with clenbuterol and recombinant human IGF1 results in additional increases in survival in male null mice. Collectively, our data support a role for IGF1 and other growth factor deficits as an underlying mechanism of Rett syndrome and introduce β2-adrenergic receptor agonists as potential therapeutic agents for the treatment of the disorder.

let-7f | LIN28A

Rett syndrome (RTT) is characterized by cognitive, behavioral, motor, and autonomic nervous system disturbances that appear after a relatively normal early postnatal time period (1, 2). More than 90% of subjects diagnosed with RTT carry mutations in methyl-CpG–binding protein 2 (*MECP2*), a gene located on the X chromosome (3). Because the vast majority of *MECP2* mutations are de novo and paternally inherited, RTT is found predominantly in females. Due to X-chromosome inactivation and mutation differences in the *MECP2* gene, patients with RTT display pronounced variability in the severity of their clinical symptoms (4). Previous studies have demonstrated that *Mecp2* knockout (KO) mice show many of the symptoms of female patients with a similar age of onset (5, 6). Female *Mecp2* heterozygous mice display a delayed and more variable phenotype, but are important for determining the sex-specific effects and preclinical value of potential therapeutic interventions (7–9). Multiple studies have reported a plethora of physiological alterations in RTT patients and *Mecp2* KO mice, including deficits in the modulation of adrenergic production and neurosecretion (10–14).

MeCP2 is involved in an extensive range of molecular functions, including influencing transcription by recruiting different chromatin-regulating complexes to the promoter region of numerous genes, promoting alternative splicing, affecting imprinting, and maintaining global chromatin structures (15). In addition, MeCP2 plays a prominent role in regulating the expression of microRNAs (miRNAs), a subset of evolutionarily conserved small noncoding RNAs that posttranscriptionally target more than half of all protein-coding genes and play an instrumental role in brain plasticity and disease (16–18). Several studies have revealed

an intriguing interplay between MeCP2 and miRNAs that regulate brain-derived neurotrophic factor (BDNF) (16–18), a molecule whose genetic overexpression can improve phenotypes in a mouse model of RTT (19).

Another growth factor recently shown to be important for RTT is insulin-like growth factor 1 (IGF1), which can partially rescue disease-related symptoms when administered to *Mecp2* KO mice in full-length form (20) or as an active tripeptide fragment (21). Indeed, several studies have demonstrated that IGF1 can rescue molecular signaling, structural and physiological phenotypes in human induced pluripotent stem cell-derived neurons (22, 23) and astrocytes (24), and clinical trials of recombinant human IGF1 for RTT have shown favorable safety (25), and safety plus efficacy (26, 27) profiles.

Here, we report that chronic treatment of young *Mecp2*-null mice with the β2-adrenergic receptor agonist clenbuterol increases survival and ameliorates respiratory, social, and motor behavioral deficits characteristic of RTT. Importantly, 3–4 wk of clenbuterol treatment in older symptomatic female *Mecp2* heterozygous mice results in additional improvement of multiple behavioral deficits. Furthermore, we report alterations in a miRNA-mediated molecular pathway that bridges the observed deficits in BDNF and IGF1 expression in the brain of male *Mecp2* mutant mice, which is also responsive to clenbuterol

Significance

Rett syndrome is a devastating neurodevelopmental disorder with diverse symptoms and no available treatment. Previous work from our laboratory has identified deficits in insulin-like growth factor 1 (IGF1) levels in *Mecp2* mutant mice, and demonstrated correction of symptoms and molecular-signaling alterations with IGF1 treatment. Here, we show that treatment with the adrenergic receptor agonist clenbuterol rescues a microRNA pathway that underlies IGF1 expression, improves survival, and ameliorates diverse phenotypes in *Mecp2* mutant mice. Life span measurements suggest that cotreatment with clenbuterol and IGF1 may further enhance their therapeutic effects in the mouse model of the disease. We would like to strongly caution, however, against any use of clenbuterol before clinical trials establish its safety and efficacy in Rett syndrome.

NEUROSCIENCE

treatment. Finally, we show that coadministration of clenbuterol and recombinant human IGF1 (rhIGF1) results in a robust boost in the survival of *Mecp2* KO mice.

Results

Clenbuterol Increases Survival, Rescues Respiratory Deficiency, and Improves Motor Coordination in Male *Mecp2*-Null Mice. Given the known abnormalities in adrenergic synthesis in RTT (10–14), we decided to test the effect on survival and behavior of chronic treatment with clenbuterol, a specific β2-adrenergic receptor agonist. In addition to its ability to effectively cross the blood–brain barrier, clenbuterol can increase BDNF levels in the brain (28) and has been reported to improve cognition, mediate neuroprotection, and reduce neuroinflammation (29–31). We therefore postulated that clenbuterol could exert therapeutic effects in *Mecp2* mouse models of RTT. Toward that end, we injected intraperitoneally (i.p.) clenbuterol (KOt), or vehicle (KOv) in male postnatal day 14 (P14) *Mecp2*$^{-/y}$ littermates, an age that is old enough to allow i.p. injections, and continued treatment until 8–9 wk or as long as the mice survived (Fig. 1*A*) (*Materials and Methods*). We initially chose a dose of 5 mg/kg, known to be effective in the brain (31).

Notably, KOt mice displayed a significant increase in survival in comparison with their littermate KOv mice (Fig. 1*B*). Of note,

treatment with 50 times lower concentration of clenbuterol, which has also been shown to affect the brain (32), still resulted in a significant increase in survival, thus expanding the range of the effective clenbuterol dose (Fig. S1 *A* and *B*).

Mecp2 KO mice are known to exhibit aberrant motor coordination, a deficit related to cerebellar BDNF levels (33). As expected, 7-wk-old KO mice showed significantly reduced performance in the rotarod assay on both the first and second experimental days (Fig. 1*C* and Fig. S2*A*). Clenbuterol significantly improved the phenotype during the second but not first day of testing (Fig. 1*C* and Fig. S2*A*), implying a modest effect on motor coordination in *Mecp2*-null mice. However, clenbuterol did not improve general locomotion in 4-wk male KO mice (Fig. S2*B*), suggesting that not all motor disturbances were ameliorated.

Previous studies have observed deficiencies in adrenergic signaling in central respiratory centers (13, 34), which are related to alterations in cyclic adenosine monophosphate (cAMP), protein kinase A (PKA), and cAMP response element-binding protein (CREB) phosphorylation (35) that are downstream of β2-adrenergic receptor signaling (29, 36). Consistent with relatively normal early development, no significant changes in respiratory frequency were observed at 4 wk (Fig. S3*A*). However, a significant deficit was found at 8 wk in KOv mice, which was rescued in clenbuterol-treated animals (Fig. 1*D*). Heart rate in KOv mice similarly showed no changes at 4 wk compared with WTv littermates, but did show a significant reduction at 8 wk (Fig. S3 *B* and *C*). However, heart rate in KOt mice was similar to that of KOv mice (Fig. S3 *B* and *C*).

We then assayed sociability and social memory in *Mecp2*$^{-/y}$ mice with the three-chamber test. Our results revealed that, although the percentage of time spent in the stimulus mouse chamber during the social approach was the same in both 7-wk-old KOv and WTv mice, KOv mice had diminished ability to recognize this previous social interaction (Fig. 1*E*). Notably, clenbuterol treatment rescued this deficit (Fig. 1*E*). Together, our data demonstrate that clenbuterol is able to enhance survival and improve multiple phenotypes in male null mice.
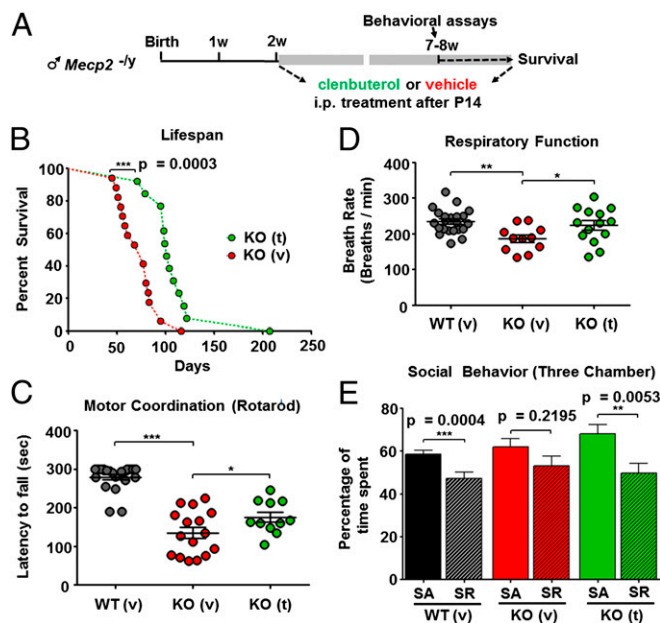
Short-Term Clenbuterol Treatment in Symptomatic Female *Mecp2*$^{-/+}$ Mice Rescues Multiple Behavioral Deficits. Experiments in female mice are necessary to preclinically evaluate the effectiveness of potential therapies related to patients with RTT who are predominately female (9). We, therefore, examined the effect of clenbuterol treatment (5 mg/kg, i.p.) in older (6–12 mo) symptomatic *Mecp2*$^{-/+}$ mice. Given the known variability in disease severity in female heterozygous mice, we measured the performance of each mouse in five behavioral assays before and after 3 or 4 wk of clenbuterol treatment, and at the same time assayed the performance of female WT mice on the same tests to discover whether any clear deficits exist in certain behaviors (Fig. 2*A*).

We first used whole-body plethysmography to measure respiratory function, including the existence of episodes of apnea. Indeed, female *Mecp2*$^{-/+}$ mice before treatment had significantly more apneas than female WT mice of similar age (Fig. 2*B*), which was rescued by clenbuterol treatment (Fig. 2*B*). Previous work has identified that the increased appearance of apneas is accompanied by enhanced postinspiratory activity in *Mecp2*-null mice (37). Indeed, significant increases in expiratory and decreases in inspiratory times were observed in pretreatment *Mecp2*$^{-/+}$ mice relative to WT female controls, which were notably reversed following clenbuterol treatment (Fig. 2 *C* and *D*). These results suggest that even short duration of clenbuterol treatment is sufficient to significantly improve respiratory function in symptomatic females.

Previous detailed analysis of the cognitive symptomatology of female *Mecp2* heterozygous mice uncovered a significant deficit in object discrimination (8). Given that clenbuterol has been shown to improve memory performance (29, 30), we repeated a

Fig. 1. Treatment with clenbuterol substantially increases survival and improves behavior of *Mecp2* KO mice. (*A*) Schematic showing the duration of clenbuterol treatment and time of behavioral assays in *Mecp2*$^{-/y}$ mice. (*B*) Graph showing cumulative survival distributions for KO vehicle [KO (v), red circles], and KO clenbuterol-treated [KO (t), green circles] mice. *P* value shown in graph is based on Gehan–Breslow–Wilcoxon test. (*C*) Graph showing mean ± SEM latency to fall rotarod motor coordination test values (in seconds) in WT vehicle [WT (v), black circles], KO vehicle [KO (v), red circles], and clenbuterol-treated [KO (t), green circles] mice during the second experimental day. (*D*) Graph showing mean ± SEM breath rate values (breaths per minute) for the three experimental groups. Stars in *C* and *D* depict statistical significance based on ANOVA with Newman–Keuls test for multiple comparisons (***P < 0.001, **P < 0.01, *P < 0.05). (*E*) Graph showing mean ± SEM percentage of time spent in the chamber with the Stimulus mouse for WT (v) (n = 29), KO (v) (n = 9), and KO (v) (n = 11) during the first (social approach or SA, filled bars) and second day (social recognition or SR, bars with diagonal lines) of the three-chamber test. The asterisks denote statistical significance based on two-tailed paired *t* test (***P < 0.001, **P < 0.01, with the exact *P* values depicted in the figure).
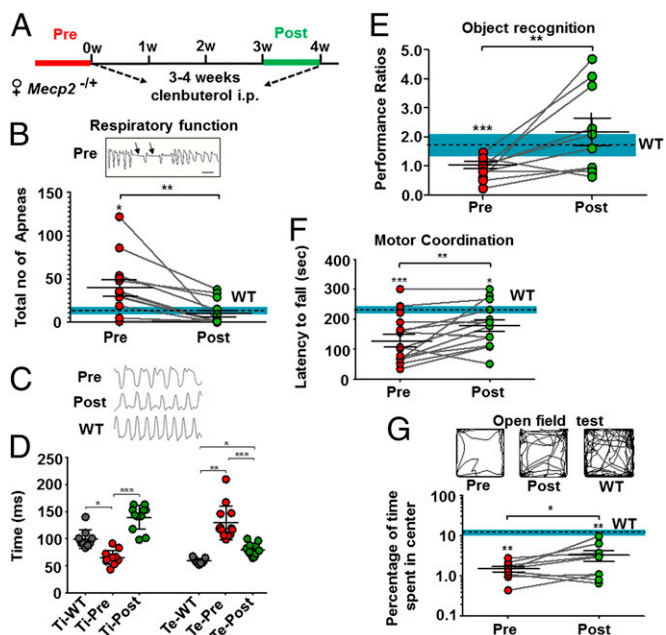
Fig. 2. Treatment with clenbuterol improves multiple behavioral deficits in symptomatic *Mecp2⁻/⁺* mice. (*A*) Schematic showing the duration of clenbuterol treatment and time of behavioral assays in *Mecp2⁻/⁺* mice. (*B, Upper*) Representative 5-s trace from a *Mecp2⁻/⁺* mouse before clenbuterol treatment showing characteristic (>0.5 s, black arrows) episodes of apnea. (Scale bar, 0.5 s.) (*Lower*) Graph showing the total number of apneas during 12-min plethysmography sessions in *Mecp2⁻/⁺* mice before (filled red circles) and after (filled green circles) 3 wk of clenbuterol treatment. (*C*) Representative 5-s respiratory traces pre- and post-clenbuterol treatment of the same *Mecp2⁻/⁺* mouse, as well as a WT control. (*D*) Graph showing mean ± SEM inspiratory (Ti) and expiratory (Te) times in milliseconds following plethysmography in *Mecp2⁻/⁺* mice before and after 3 wk of clenbuterol treatment, as well as in WT female mice. Stars depict statistical significance based on Kruskal–Wallis ANOVA with Dunn's multiple-comparison test (***$P <$ 0.001, **$P <$ 0.01, *$P <$ 0.05). (*E*) Graph showing the object recognition performance ratio (*SI Materials and Methods*) before and after 3–4 wk of clenbuterol treatment. (*F*) Graph showing latency to fall rotarod motor coordination test values (in seconds) before and after 4 wk of clenbuterol treatment. Results from the first experimental day are shown. (*G, Upper*) Representative traces from the open field assay for the same female *Mecp2⁻/⁺* mouse pre- and post-clenbuterol treatment and for a WT female control mouse. (*Lower*) Graph showing the percentage of time spent in the center of the arena before (pre, red filled circles) and after (post, green filled circles) 3 wk of daily clenbuterol treatment in female *Mecp2⁻/⁺* mice. In all graphs but *D*, stars between treatments depict statistical significance (**$P <$ 0.01, *$P <$ 0.05) based on two-tailed paired Student *t* test (*E* and *F*) or Wilcoxon matched-pairs signed rank test (*B* and *G*), and stars over data points depict significance relative to WT female mice based on two-tailed one-sample Student *t* test (*E* and *F*), or two-tailed Wilcoxon signed rank test (*B* and *G*) (***$P <$ 0.001, *$P <$ 0.05). In graphs *B*, *E*, *F*, and *G*, the dotted lines and blue shading depict the mean ± SEM values of female WT control mice.

similar behavioral assay before and after 3–4 wk of clenbuterol treatment. Indeed, *Mecp2⁻/⁺* mice exhibited a significant disturbance relative to WT female mice in recognizing the rearrangement of two objects inside an arena (Fig. 2*E*) (*SI Materials and Methods*). Intriguingly, clenbuterol abolished the observed deficit in object recognition, suggesting that it could be effective in improving cognitive alterations in female *Mecp2⁺/⁻* mice (Fig. 2*E*).

In addition, clenbuterol treatment in female heterozygous mice resulted in an amelioration of the motor coordination deficits, which was apparent in both days of testing (Fig. 2*F* and Fig. S4*A*). However, given the known suppressive effects of high clenbuterol dosage through binding to peripheral adrenergic

receptors (38), we did not observe any improvements on total distance traveled by the mice after treatment (Fig. S4*B*). Similarly, and in agreement with results in null males, clenbuterol treatment in female *Mecp2⁻/⁺* mice did not improve the total crossings in the locomotor behavioral assay (Fig. S4*C*).

Last, heterozygous female mice exhibited increased anxiety in the open field test relative to WT female controls, as shown by a low percentage of the time spent in the center of the test arena (Fig. 2*G*). Clenbuterol treatment significantly increased the relative time spent in the center, although the anxiolytic effect after treatment was modest. Collectively, our data suggest that short-term treatment with clenbuterol in symptomatic female heterozygous mice exerts significant improvements in multiple behavioral phenotypes related to RTT.

IGF1 Is Reduced in *Mecp2* Mutant Mice Through a miRNA-Mediated Mechanism and Restored by Clenbuterol. To dissect the molecular pathways that could be downstream of clenbuterol, we measured levels of BDNF and related downstream molecules in the cerebellum, a brain region severely affected by the disease (39, 40), of male KOv and KOt mice and their WT littermates (animals were injected daily with saline vehicle or 5 mg/kg clenbuterol from P14 to 8–9 wk of age). Clenbuterol-mediated activation of β2-adrenergic receptors in the brain is known to activate PKA, thereby phosphorylating and activating CREB (29, 32). As predicted, due to the high relative abundance of β2-adrenergic receptors in the cerebellum (41), the ratio of activated to total CREB (pCREB/tCREB) was significantly increased after clenbuterol treatment (Fig. 3*A*). Given that MeCP2 affects BDNF transcription through mechanisms including CREB signaling (16, 42), we measured BDNF expression. Indeed, levels of both cerebellar BDNF mRNA and protein were reduced in KOv mice relative to WT controls but significantly increased in KOt mice, suggesting that clenbuterol can ameliorate the alterations in BDNF expression observed in *Mecp2* KO mice (Fig. 3 *B* and *C*).

A recent study had suggested that BDNF can regulate the protein levels of miRNA-processing factor Lin-28 homolog A (LIN28A) (43), a protein known to affect the maturation of the let-7 family of miRNAs (44). We found a greater than twofold reduction in LIN28A protein in the cerebellum of *Mecp2* KO mice, suggesting that miRNA processing might be perturbed (Fig. 3*D*). LIN28A specifically inhibits the let-7 miRNAs (44), and we found that multiple members of the let-7 family were increased, with let-7f showing the most robust increase (Fig. 3*E* and Fig. S5*A*). Intriguingly, clenbuterol treatment completely rescued LIN28A protein (Fig. 3*D*) and let-7f mature miRNA levels (Fig. 3*E*). The effect of LIN28A on let-7f is not expected to influence the processing of initial nuclear primary precursor miRNA (pri-miRNA) (44); consistently, we found no changes in the expression of the two pri-miRNAs that produce identical, in sequence, mature let-7f molecules (Fig. S5*B*).

It has been previously shown that let-7f can inhibit IGF1 expression in rat microglia (45). Because IGF1 protein is highly expressed in the serum and can easily cross the blood–brain barrier in an activity-dependent manner (46), we measured cerebellar IGF1 mRNA expression. Our data revealed a significant reduction in local IGF1 mRNA levels in KO mice (Fig. 3*F*), suggesting that brain-specific IGF1 synthesis may be perturbed in RTT. Importantly, treatment with clenbuterol led to significant increase in cerebellar IGF1 mRNA levels as well (Fig. 3*F*).

In addition to its impact on BDNF expression, clenbuterol has been reported by multiple studies to increase the levels of nerve growth factor (NGF) (28, 32), a protein known to be reduced in the striatum of *Mecp2* KO mice (47). Our results showed that, although NGF is not reduced in KO vehicle mice, both mRNA and protein levels were significantly increased following clenbuterol treatment (Fig. S6 *A* and *B*).
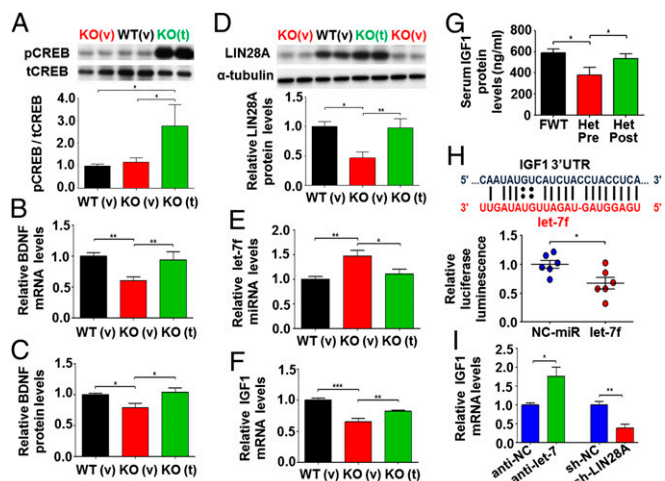
NEUROSCIENCE

Fig. 3. A miRNA-mediated pathway controlling IGF1 expression is altered in *Mecp2* male null mice and restored by clenbuterol treatment. (*A, Upper*) Representative blot showing levels of phosphorylated CREB (pCREB) normalized to total CREB (tCREB) WT vehicle [WT (v), black bars; *n* = 7], KO vehicle [KO (v), red bars; *n* = 6], and clenbuterol-treated [KO (t), green bars; *n* = 5] mice. (*Lower*) Graph showing mean ± SEM cerebellar pCREB/tCREB ratio based on Western blotting. (*B* and *C*) Graphs showing mean ± SEM cerebellar BDNF mRNA levels based on quantitative real-time PCR (*B*), and BDNF protein levels based on ELISA (*C*). Number of samples for WT (v), KO (v), and KO (t) were 12, 9, and 8, respectively for mRNA and 9, 8, and 8 for protein levels. (*D, Upper*) Representative blot showing levels of LIN28A normalized to α-tubulin for the three groups of mice described in *A*. (*Lower*) Graph showing mean ± SEM normalized cerebellar LIN28A protein levels for WT (v) (*n* = 7), KO (v) (*n* = 5), and KO (v) (*n* = 5). (*E* and *F*) Graphs showing mean ± SEM cerebellar mature let-7f miRNA (*E*) and IGF1 mRNA (*F*) levels in WT (v) (*n* = 12), KO (v) (*n* = 9), and KO (t) (*n* = 8) mice. The stars in graphs *A–F* depict statistical significance based on ANOVA with Newman–Keuls test for multiple comparisons (**P < 0.01, *P < 0.05, comparing WTv vs. KOv and KOt vs. KOv). (*G*) Graph showing mean ± SEM serum IGF1 protein levels (in nanograms per milliliter) based on ELISA in female WT mice (FWT, filled black bars; *n* = 10) and *Mecp2*$^{+/-}$ mice before (HET pre, filled red bars; *n* = 9) and after (HET post, filled green bars; *n* = 9) clenbuterol treatment for 4 wk. The stars (*P < 0.05) depict significance based on ANOVA with Newman–Keuls multiple-comparison test. (*H, Upper*) Predicted interaction between let-7f miRNA (red) and mouse IGF1-1 3′-UTR sequences (black). The bars represent canonical Watson–Crick base pair and the double dots depict G-U wobble base pairing. (*Lower*) Graph showing mean ± SEM relative luminescence in let-7f and negative control miRNA (NC-miR) precursor transfected HEK293 cells expressing luciferase fused to mouse IGF1 3′-UTR. Relative luminescence was calculated by dividing firefly to *Renilla* luciferase, and all values were transformed to ratios relative to NC-miR. (*I*) Graph showing mean ± SEM relative to negative controls (anti-NC for miRNA inhibitor and sh-NC for shRNA control) or sIGF1 mRNA levels in Hep G2 cells after let-7f inhibition (anti-let-7f; *n* = 5) and shRNA-mediated knockdown of LIN28A (sh-LIN28A; *n* = 5). The stars in *H* and *I* depict statistical significance (**P < 0.01, *P < 0.05) based on two-tailed Student *t* test.

Given that brain measurements were not possible in female heterozygous mice because the same mice were used for before- and after-treatment comparison, and because serum IGF1 protein levels are reduced in male *Mecp2*-null mice (20), we examined IGF1 protein levels in the serum of female *Mecp2*$^{-/+}$ mice before and after treatment with clenbuterol. Indeed, serum IGF1 protein expression was reduced relative to WT female mice in the *Mecp2*$^{-/+}$ mice before treatment (Fig. 3*G*) and was restored following 4 wk of clenbuterol treatment (Fig. 3*G*).

The sequence of let-7f is predicted to be complementary to an evolutionarily conserved region in the 3′-untranslated region (3′-UTR) of IGF1 mRNA (Fig. 3*H*). To validate a direct interaction, we added a large fragment of mouse IGF1 3′-UTR containing the let-7f predicted target site downstream of the luciferase gene and

compared relative luminescence after overexpressing let-7f in HEK293 cells. Our results showed that transfection with synthetic let-7f precursors increased mature let-7f levels relative to miRNA precursor negative control (P = 0.0043, Mann–Whitney test) and significantly reduced luciferase activity (Fig. 3*H*). To further test the effects of LIN28A and let-7f on IGF1 expression, we transfected a human hepatocyte carcinoma cell line (Hep G2) with shRNAs against LIN28A and miRNA inhibitors against let-7f together with scrambled negative miRNA and shRNA controls. Our results showed that Hep G2 cells express let-7f and LIN28A, both of which are inhibited following miRNA inhibition and shRNA-mediated knockdown, respectively ([Fig. S7]). Intriguingly, levels of human IGF1 mRNA significantly increased following inhibition of let-7f (Fig. 3*I*). However, knockdown of LIN28A, which is known to inhibit let-7 miRNAs, resulted in a robust reduction in IGF1 mRNA (Fig. 3*I*), suggesting that altered expression of LIN28A and let-7f can differentially influence IGF1 levels.

To examine whether the differential expression of the multiple components of the molecular pathway downstream of BDNF were associated with each other, we compared mRNA/miRNA and protein expression in the same male WT and KOv and KOt mice. This revealed a significant positive correlation between BDNF mRNA and LIN28A protein (Fig. 4*A*), and significant negative correlations between LIN28A/let-7f and let-7f/IGF1 (Fig. 4 *B* and *C*). Taken together, these data suggest that a complex miRNA-mediated molecular pathway downstream of MeCP2 can be linked to reduced BDNF and IGF1 expression in brain and serum of *Mecp2* mutant mice, which can be restored in vivo following treatment with clenbuterol (Fig. 4*D*).

Combinatorial Treatment with Clenbuterol and rhIGF1 Increases Survival and Further Improves the Phenotype of *Mecp2* KO Mice. Because clenbuterol resulted in a partial rescue of IGF1 expression, the restoration of BDNF, and an increase in NGF levels, we reasoned that combining clenbuterol treatment with IGF1 supplementation might result in an additive therapeutic
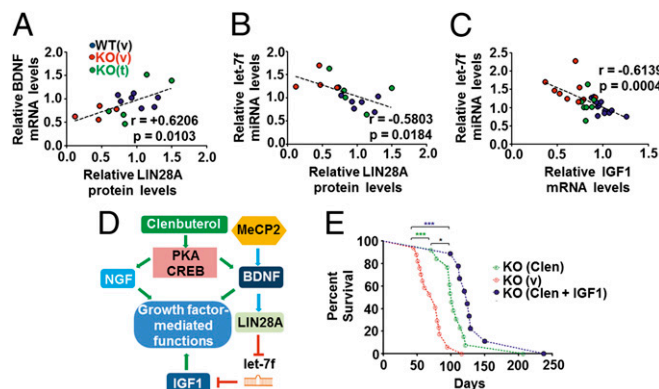

Fig. 4. Clenbuterol-mediated restoration of brain growth factor expression and synergistic effects with rhIGF1 in male *Mecp2*-null mice. (*A–C*) Graphs showing sample-by-sample correlation between (*A*) BDNF mRNA and LIN28A protein levels, (*B*) mature let-7f miRNA levels with LIN28A protein, as well as (*C*) IGF1 mRNA expression. Colors depict sample identity [blue for WT (v), green for KO (t), and red for KO (v) mice]. (*D*) Schematic depicting the proposed molecular mechanism linking Mecp2-regulated BDNF to IGF1 through LIN28A and IGF1. The effect of clenbuterol treatment in restoring NGF and BDNF levels through CREB activation and indirectly affecting IGF1 expression, thus regulating growth factor-mediated functions, is also shown. (*E*) Graph showing cumulative survival distributions for *Mecp2* KO mice receiving clenbuterol and rhIGF1 cotreatment [KO (Clen + IGF1), blue circles]. Survival of KO vehicle [KO (v), open red circles] and clenbuterol-treated [KO (clen), open green circles] mice is also depicted for comparison (from Fig. 1*A*). The stars represent statistical significance based on Gehan–Breslow–Wilcoxon test (***P < 0.001, *P < 0.05).

effect. We thus cotreated animals with clenbuterol and rhIGF1, a drug that is in clinical trials for its therapeutic effects on RTT patients (25–28).

Notably, rhIGF1-plus-clenbuterol–treated *Mecp2* KO mice (double-treated mice) displayed a robust increase in survival in comparison with KOv, which was significantly greater than clenbuterol monotherapy (Fig. 4*E*). As rhIGF1 administration alone in *Mecp2* KO mice results in a small but significant increase in survival (20), the larger improvement in survival observed in double-treated mice is most likely explained by a synergistic effect between the two treatments. In addition, double-treated KO mice exhibited a modest but significant increase in total body weight compared with clenbuterol monotherapy, although body weight was still much lower than in WT mice (Fig. S8*A*). Last, double-treated mice further increased their breath and cardiac rates at 4 wk relative to clenbuterol alone, but not at 8 wk where the deficit relative to WT mice is apparent (Fig. S8 *B* and *C*), suggesting that the synergistic effect on survival is less likely to be attributed to changes in respiratory and cardiac frequency. We conclude that coadministration of clenbuterol and rhIGF-1 contributes to additional improvements in the survival of *Mecp2* KO mice.

Discussion

Although RTT is a primarily monogenic disorder, MeCP2 modulates a plethora of molecular pathways, making it challenging to uncover an effective mechanism-based treatment (15, 48). The partial success of rhIGF1 in restoring numerous behavioral and organismal functions disrupted in *Mecp2* KO mice (20), the safety and efficacy of rhIGF1 in clinical trials (25–28), as well as the ability of rhIGF1 to rescue neuronal phenotypes in patient-derived neurons (22, 23) and astrocytes (24), prompted us to investigate whether *Mecp2* knockdown can affect IGF1 expression, and look into additional drugs with potential to mechanistically rescue deficiencies in brain growth factor expression. Here, we show that, in addition to the known deficits in BDNF expression, IGF1 synthesis is reduced in the cerebellum of male *Mecp2* KO mice, which is associated with a decreased level of miRNA-processing gene LIN28A and an up-regulation of LIN28A-regulated let-7f miRNA. Notably, we show that knockdown of LIN28A, which is known to be downstream of BDNF (43), increases IGF1 expression, whereas inhibition of let-7f reduces IGF1 expression in a human cell line. Treatment with the β2-adrenergic receptor agonist clenbuterol can restore BDNF mRNA, LIN28A, and mature let-7f levels, and can significantly augment IGF1 mRNA expression in the cerebellum of *Mecp2* KO mice. Importantly, we demonstrate that clenbuterol is able to increase survival, rescue respiratory and social abnormalities, and improve motor coordination in male *Mecp2*-null mice. In addition, treatment of older female heterozygous mice with clenbuterol for a short duration of time results in notable improvements in respiratory function and motor coordination and restores cognitive function while reducing anxiety. Furthermore, combination treatment of clenbuterol with rhIGF1 results in a more robust amelioration of survival in *Mecp2* KO mice.

Previous studies have revealed a disruption in monoamine synthesis and secretion in RTT; this causes respiratory abnormalities and reduced survival (13). Furthermore, it has been proposed that respiratory brainstem networks have a disruption in cAMP/PKA/CREB signaling (35). Because β2-adrenergic receptor activation engages the same molecular pathway (29, 36), it could be related to clenbuterol's positive effect on respiratory function. In addition, treatment with desipramine, which inhibits the reuptake of adrenaline and serotonin, has proven effective in restoring respiratory function (49). It is unclear, however, whether improvements in respiratory function following clenbuterol treatment are a result of its effects on BDNF signaling, whose pharmacological activation leads to significant amelioration of

respiratory dysfunction in the animal model of RTT (50). It should be noted, also, that despite the clear deficiency in breathing frequency in *Mecp2* KO mice known to be part of a general respiratory depression phenotype (51) and the frequent apneas and deficits in respiratory rhythm detected in female heterozygous mice through whole-body plethysmography, respiratory dysfunction in RTT patients is complex and is often complicated by frequent aspiration and gastroesophageal reflux.

Despite the fact that BDNF–LIN28A, LIN28A–let-7, and let-7f–IGF1 interactions have independently been verified in different systems (43–45), our study provides additional in vivo correlative and in vitro mechanistic evidence of a linear pathway downstream of BDNF that involves all four molecular components (Fig. 4*D*). However, we cannot exclude any parallel nonlinear interactions between any of these four genes affected by *Mecp2* knockdown and responding to clenbuterol treatment, especially given the known interplay between BDNF and IGF1 signaling (52). Future studies using BDNF, *Lin28a,* and *Let7f* knockout or transgenic mice are needed to further elucidate this mechanistic model in vivo, which could be of importance for understanding RTT therapeutics.

In addition to the beneficial effects on survival and behavior, clenbuterol has a potent anticonvulsant effect (31). Although not examined in our study, this could be significant given the high prevalence of epilepsy in RTT patients (53). Additionally, clenbuterol has been shown to block sodium channels (31), whose overactivity is hypothesized to result in the lethal cardiac arrhythmias present in RTT (54).

Clenbuterol is approved as a bronchodilator in some countries but is only designated for veterinary treatment of asthma in the United States. Our data suggest a previously unidentified potential use for β2-adrenergic receptor agonists such as clenbuterol for the treatment of RTT, either alone or in combination with rhIGF1. It has to be noted, however, that despite the fact that clenbuterol was well tolerated in the mice tested in this study, it has serious side effects especially at high dosages in humans (55). Moreover, it should be emphasized that the dosage used in our study is prohibited for clinical applications, which in conjunction with the fact that clenbuterol is not approved in all countries for human use due to its side effects and misuse as a performance enhancing drug, should encourage further research on finding new β2-adrenergic receptor agonists that can cross the blood–brain barrier yet are characterized by a better therapeutic index in comparison with clenbuterol.

Last, information on the pharmacokinetics, safety, and efficacy of a drug in the general population may not predict how individuals with serious illness such as RTT will respond even in low presumed-safe doses. Thus, careful controlled studies will be required before these findings can be applied to humans; hence we strongly caution against any use of clenbuterol outside clinically approved applications.

Materials and Methods

Male *Mecp2*$^{-/y}$ and female *Mecp2*$^{-/+}$ mice and WT littermates used in our study were obtained by breeding heterozygous females of C57BL/6 background (5) with WT C57BL/6 male mice. Both vehicle (saline)-, clenbuterol-, and clenbuterol-plus-rhIGF1–treated male animals were i.p. injected daily for 5 d, followed by a 2-d off period, repeated weekly, with 5 or 0.1 mg/kg of clenbuterol hydrochloride (Sigma-Aldrich) or vehicle starting on P14 until the animal's death/euthanasia. Intraperitoneal injection of a mix of 0.25 mg/kg full-length rhIGF1 (Peprotech)—a dose that is equivalent of the Food and Drug Administration-approved dose—and 5 mg/kg clenbuterol was also used for cotreatment experiments. Adult (6- to 12-mo-old) heterozygous females of the same C57BL/6 background and parents (5) were also treated with 5 mg/kg clenbuterol daily for 4 wk. All animal experimental protocols adhered to the National Institutes of Health's *Guide for the Care and Use of Laboratory Animals* (56) and were approved by the Animal Care and Use Committee at Massachusetts Institute of Technology.

Additional methods are provided in *SI Materials and Methods.*

1. Chahrour M, Zoghbi HY (2007) The story of Rett syndrome: From clinic to neurobiology. *Neuron* 56(3):422–437.
2. Neul JL, et al.; RettSearch Consortium (2010) Rett syndrome: Revised diagnostic criteria and nomenclature. *Ann Neurol* 68(6):944–950.
3. Amir RE, et al. (1999) Rett syndrome is caused by mutations in X-linked MECP2, encoding methyl-CpG-binding protein 2. *Nat Genet* 23(2):185–188.
4. Ishii T, et al. (2001) The role of different X-inactivation pattern on the variable clinical phenotype with Rett syndrome. *Brain Dev* 23(Suppl 1):S161–S164.
5. Guy J, Hendrich B, Holmes M, Martin JE, Bird A (2001) A mouse Mecp2-null mutation causes neurological symptoms that mimic Rett syndrome. *Nat Genet* 27(3):322–326.
6. Ricceri L, De Filippis B, Laviola G (2008) Mouse models of Rett syndrome: From behavioural phenotyping to preclinical evaluation of new therapeutic approaches. *Behav Pharmacol* 19(5-6):501–517.
7. Samaco RC, et al. (2013) Female Mecp2(+/−) mice display robust behavioral deficits on two different genetic backgrounds providing a framework for pre-clinical studies. *Hum Mol Genet* 22(1):96–109.
8. Stearns NA, et al. (2007) Behavioral and anatomical abnormalities in Mecp2 mutant mice: A model for Rett syndrome. *Neuroscience* 146(3):907–921.
9. Katz DM, et al. (2012) Preclinical research in Rett syndrome: Setting the foundation for translational success. *Dis Model Mech* 5(6):733–745.
10. Ide S, Itoh M, Goto Y (2005) Defect in normal developmental increase of the brain biogenic amine concentrations in the mecp2-null mouse. *Neurosci Lett* 386(1):14–17.
11. Samaco RC, et al. (2009) Loss of MeCP2 in aminergic neurons causes cell-autonomous defects in neurotransmitter synthesis and specific behavioral abnormalities. *Proc Natl Acad Sci USA* 106(51):21966–21971.
12. Taneja P, et al. (2009) Pathophysiology of locus ceruleus neurons in a mouse model of Rett syndrome. *J Neurosci* 29(39):12187–12195.
13. Viemari JC, et al. (2005) MeCP2 deficiency disrupts norepinephrine and respiratory systems in mice. *J Neurosci* 25(50):11521–11530.
14. Zoghbi HY, Percy AK, Glaze DG, Butler IJ, Riccardi VM (1985) Reduction of biogenic amine levels in the Rett syndrome. *N Engl J Med* 313(15):921–924.
15. Castro J, Mellios N, Sur M (2013) Mechanisms and therapeutic challenges in autism spectrum disorders: Insights from Rett syndrome. *Curr Opin Neurol* 26(2):154–159.
16. Klein ME, et al. (2007) Homeostatic regulation of MeCP2 expression by a CREB-induced microRNA. *Nat Neurosci* 10(12):1513–1514.
17. Wu H, et al. (2010) Genome-wide analysis reveals methyl-CpG-binding protein 2-dependent regulation of microRNAs in a mouse model of Rett syndrome. *Proc Natl Acad Sci USA* 107(42):18161–18166.
18. Mellios N, Sur M (2012) The emerging role of microRNAs in schizophrenia and autism spectrum disorders. *Front Psychiatry* 3:39.
19. Chang Q, Khare G, Dani V, Nelson S, Jaenisch R (2006) The disease progression of Mecp2 mutant mice is affected by the level of BDNF expression. *Neuron* 49(3):341–348.
20. Castro J, et al. (2014) Functional recovery with recombinant human IGF1 treatment in a mouse model of Rett syndrome. *Proc Natl Acad Sci USA* 111:9941–9946.
21. Tropea D, et al. (2009) Partial reversal of Rett Syndrome-like symptoms in MeCP2 mutant mice. *Proc Natl Acad Sci USA* 106(6):2029–2034.
22. Marchetto MC, et al. (2010) A model for neural development and treatment of Rett syndrome using human induced pluripotent stem cells. *Cell* 143(4):527–539.
23. Li Y, et al. (2013) Global transcriptional and translational repression in human-embryonic-stem-cell-derived Rett syndrome neurons. *Cell Stem Cell* 13(4):446–458.
24. Williams EC, et al. (2014) Mutant astrocytes differentiated from Rett syndrome patients-specific iPSCs have adverse effects on wild-type neurons. *Hum Mol Genet* 23(11):2968–2980.
25. Pini G, et al. (2012) IGF1 as a potential treatment for Rett syndrome: Safety assessment in six Rett patients. *Autism Res Treat* 2012:679801.
26. Ho E, et al. (2012) Initial study of rh-IGF1 (mecasermin [DNA] injection) for treatment of Rett syndrome and development of Rett-specific novel biomarkers of cortical and autonomic function. *Neurology* 78(Meeting Abstracts 1):S28.005.
27. Khwaja OS, et al. (2014) Safety, pharmacokinetics, and preliminary assessment of efficacy of mecasermin (recombinant human-IGF1 injection) for the treatment of Rett syndrome. *Proc Natl Acad Sci USA* 111(12):4596–4601.
28. Gleeson LC, Ryan KJ, Griffin EW, Connor TJ, Harkin A (2010) The β2-adrenoceptor agonist clenbuterol elicits neuroprotective, anti-inflammatory and neurotrophic actions in the kainic acid model of excitotoxicity. *Brain Behav Immun* 24(8):1354–1361.
29. Zhou HC, et al. (2013) Activation of β2-adrenoceptor enhances synaptic potentiation and behavioral memory via cAMP-PKA signaling in the medial prefrontal cortex of rats. *Learn Mem* 20(5):274–284.
30. Ramos BP, Colgan LA, Nou E, Arnsten AF (2008) Beta2 adrenergic agonist, clenbuterol, enhances working memory performance in aging animals. *Neurobiol Aging* 29(7):1060–1069.
31. Fischer W, Kittner H, Regenthal R, Malinowska B, Schlicker E (2001) Anticonvulsant and sodium channel blocking activity of higher doses of clenbuterol. *Naunyn Schmiedebergs Arch Pharmacol* 363(2):182–192.
32. Culmsee C, Stumm RK, Schäfer MK, Weihe E, Krieglstein J (1999) Clenbuterol induces growth factor mRNA, activates astrocytes, and protects rat brain tissue against ischemic damage. *Eur J Pharmacol* 379(1):33–45.
33. Kondo M, et al. (2008) Environmental enrichment ameliorates a motor coordination deficit in a mouse model of Rett syndrome—Mecp2 gene dosage effects and BDNF expression. *Eur J Neurosci* 27(12):3342–3350.
34. Kerr AM (1992) A review of the respiratory disorder in the Rett syndrome. *Brain Dev* 14(Suppl):S43–S45.
35. Mironov SL, Skorova EY, Kügler S (2011) Epac-mediated cAMP-signalling in the mouse model of Rett Syndrome. *Neuropharmacology* 60(6):869–877.
36. Li Y, et al. (2012) Clenbuterol upregulates histone demethylase JHDM2a via the β2-adrenoceptor/cAMP/PKA/p-CREB signaling pathway. *Cell Signal* 24(12):2297–2306.
37. Stettner GM, et al. (2007) Breathing dysfunctions associated with impaired control of postinspiratory activity in Mecp2−/y knockout mice. *J Physiol* 579(Pt 3):863–876.
38. Geyer MA, Frampton SF (1988) Peripheral mediation of effects of clenbuterol on locomotor and investigatory behavior in rats. *Pharmacol Biochem Behav* 30(2):417–420.
39. Murakami JW, Courchesne E, Haas RH, Press GA, Yeung-Courchesne R (1992) Cerebellar and cerebral abnormalities in Rett syndrome: A quantitative MR analysis. *AJR Am J Roentgenol* 159(1):177–183.
40. Nag N, Mellott TJ, Berger-Sweeney JE (2008) Effects of postnatal dietary choline supplementation on motor regional brain volume and growth factor expression in a mouse model of Rett syndrome. *Brain Res* 1237:101–109.
41. Rainbow TC, Parsons B, Wolfe BB (1984) Quantitative autoradiography of beta 1- and beta 2-adrenergic receptors in rat brain. *Proc Natl Acad Sci USA* 81(5):1585–1589.
42. Abuhatzira L, Makedonski K, Kaufman Y, Razin A, Shemer R (2007) MeCP2 deficiency in the brain decreases BDNF levels by REST/CoREST-mediated repression and increases TRKB production. *Epigenetics* 2(4):214–222.
43. Huang YW, Ruiz CR, Eyler EC, Lin K, Meffert MK (2012) Dual regulation of miRNA biogenesis generates target specificity in neurotrophin-induced protein synthesis. *Cell* 148(5):933–946.
44. Piskounova E, et al. (2011) Lin28A and Lin28B inhibit let-7 microRNA biogenesis by distinct mechanisms. *Cell* 147(5):1066–1079.
45. Selvamani A, Sathyan P, Miranda RC, Sohrabji F (2012) An antagomir to microRNA Let7f promotes neuroprotection in an ischemic stroke model. *PLoS One* 7(2):e32662.
46. Nishijima T, et al. (2010) Neuronal activity drives localized blood-brain-barrier transport of serum insulin-like growth factor-I into the CNS. *Neuron* 67(5):834–846.
47. Ricceri L, De Filippis B, Fuso A, Laviola G (2011) Cholinergic hypofunction in MeCP2-308 mice: Beneficial neurobehavioural effects of neonatal choline supplementation. *Behav Brain Res* 221(2):623–629.
48. Chapleau CA, et al. (2013) Recent progress in Rett syndrome and MeCP2 dysfunction: Assessment of potential treatment options. *Future Neurol* 8(1):21–28.
49. Roux JC, Dura E, Moncla A, Mancini J, Villard L (2007) Treatment with desipramine improves breathing and survival in a mouse model for Rett syndrome. *Eur J Neurosci* 25(7):1915–1922.
50. Ogier M, et al. (2007) Brain-derived neurotrophic factor expression and respiratory function improve after ampakine treatment in a mouse model of Rett syndrome. *J Neurosci* 27(40):10912–10917.
51. Bissonnette JM, Knopp SJ (2006) Separate respiratory phenotypes in methyl-CpG-binding protein 2 (Mecp2) deficient mice. *Pediatr Res* 59(4 Pt 1):513–518.
52. Zheng WH, Quirion R (2004) Comparative signaling pathways of insulin-like growth factor-1 and brain-derived neurotrophic factor in hippocampal neurons and the role of the PI3 kinase pathway in cell survival. *J Neurochem* 89(4):844–852.
53. Glaze DG, et al. (2010) Epilepsy and the natural history of Rett syndrome. *Neurology* 74(11):909–912.
54. McCauley MD, et al. (2011) Pathogenesis of lethal cardiac arrhythmias in MeCP2 mutant mice: Implication for therapy in Rett syndrome. *Sci TransMed* 3(113):113ra125.
55. Spiller HA, James KJ, Scholzen S, Borys DJ (2013) A descriptive study of adverse events from clenbuterol misuse and abuse for weight loss and bodybuilding. *Subst Abus* 34(3):306–312.
56. Committee for the Update on the *Guide for the Care and Use of Laboratory Animals* (2011) *Guide for the Care and Use of Laboratory Animals* (The National Academies Press, Washington, DC), 8th Ed.

Supporting Information

Mellios et al. 10.1073/pnas.1309426111

SI Materials and Methods

Luciferase Assay. HEK293 (GripTite293 MSR; Life Technologies) cells were used to evaluate let-7f precursor effects on the expression levels of an insulin-like growth factor 1 (IGF1) 3′-UTR firefly luciferase reporter plasmid (miTarget 3′-UTR miRNA Target Clones; NM_001111274 3′-UTR; GeneCopoeia) also containing a separate *Renilla* luciferase reporter for normalizing transfection efficiency. Cells were cultured in HEK293 medium [DMEM plus 2 mM glutamine plus 1% nonessential amino acids (NEAA) plus 10% (mg/100mL) FBS plus 1× pen/strep] as per the vendor's recommendation. For transfection and analysis, cells were seeded in 96-well tissue culture-treated plates (BD Biosciences) at a seeding density of 10,000 cells in 100-μL volume per well in HEK293 medium without pen/strep the day before transfection. Transfection of test RNAs [mirVana hsa-let-7f PremiR precursor, and Pre-Mir Negative control #1 (Life Technologies)] and reporter plasmid [microRNA (miRNA) IGF1 3′-UTR target clone (GeneCopoeia)] was performed with Lipofectamine 2000 (Life Technologies). Nucleic acids and reagents were preincubated per the vendor's procedure resulting in 25-μL transfection mixtures per well composed of 1 μL of transfection reagent with 5 pmol of RNA and 1 μg of reporter plasmid. Transfection mixtures were added directly to 100 μL of medium in each well and incubated overnight. Medium was then replaced with HEK293 medium containing 1× pen/strep. Luciferase expression was measured using the Luc-Pair miR Luciferase Assay (GeneCopoeia) per included instructions. Firefly luciferase was measured on a Perkin-Elmer Envision Multilabel Plate Reader followed by *Renilla* luciferase per assay instructions.

HepG2 Cell Culture and Transfection. The human hepatocyte carcinoma cell line, Hep G2 (Sigma-Aldrich), was used to evaluate let-7f and Lin-28 homolog A (Lin28a) inhibition on the expression of Lin28a, IGF1, and let-7f, which are endogenously expressed at moderate levels in this line. Hep G2 cells were cultured in Hep G2 medium [Eagle's minimum essential medium plus 2 mM glutamine plus 1% NEAA plus 10% (mg/100 mL) FBS plus 1× pen/strep] as per the vendor's recommendation. For transfection and analysis, cells were seeded in 96-well tissue culture-treated plates (BD Biosciences) at a seeding density of 10,000 cells in 100-μL volume per well in Hep G2 medium without pen/strep the day before transfection. Transfection of test RNAs [mirVana hsa-let-7f-5p inhibitor or mirVana miRNA inhibitor Negative Control #1 (Life Technologies)] or plasmids [LIN28A shRNA plasmid mixture (OriGene Technologies; #TR513548) or Negative Control (#TR30015)] was performed with Lipofectamine 2000 (Life Technologies). Nucleic acids and reagent were preincubated per vendor procedure resulting in 25 μL of transfection mixtures per well composed of 1 μL of transfection reagent with either 5 pmol of RNA or 1 μg of total plasmid. Transfection mixtures were added directly to 100 μL of medium in each well and incubated overnight. Medium was then replaced with Hep G2 medium containing 1× pen/strep. Cells were harvested with TrypLE (Life Technologies), pelleted, and quick frozen on dry ice for subsequent RNA isolation and analysis.

RNA and Protein Measurements. Mice were anesthetized using isoflurane and euthanized using cervical dislocation. The two cerebellar hemispheres were isolated, placed in separate tubes, and stored at −80 °C. For RNA extraction of both mouse and human cell line RNA, the miRNeasy Mini Kit (Qiagen) was used

based on manufacturer's instructions. RNA concentration and quality was assayed using NanoDrop (Thermo Scientific). For mature miRNA measurements, 10 ng of RNA were reverse transcribed using miRNA reverse transcription kit (Life Technologies), and the product was diluted 1:15 in RNase-free water. Levels of mature miRNAs, as well as normalizer mouse snoRNA202 or human RNU44, were assayed in triplicates following quantitative real-time PCR (qRT-PCR) with Taqman qRT-PCR assays (Life Technologies) and analyzed based on the formula $C = 2^{\wedge}CTnormalizer/2^{\wedge}CTmiRNA$. Both reverse transcription and qRT-PCR miRNA primers were part of Taqman miRNA assays (Life Technologies). For mRNA and primary precursor miRNA (pri-miRNA) measurements, 300 ng of RNA were reverse transcribed using vilo cDNA kit (Invitrogen). cDNA was diluted at 1:15 for all mRNA and pri-miRNA measurements, with the exception of 18S rRNA, which required a 1:300 dilution. The geometric mean of β-actin and 18S rRNA or 18S rRNA alone for human Hep G2 cells was used for normalization using the following formula: $C = 2^{\wedge}CTnormalizer/2^{\wedge}CTmRNA$ or pri-miRNA. For brain-derived neurotrophic factor (BDNF), the primer used covered multiple alternative transcripts (variants 1–11; Taqman primer ID: Mm04230607_s1).

For protein isolation, cerebellar samples were homogenized and dissociated in RIPA buffer (Sigma) with the addition of Complete Protease Inhibitors (Roche) and PhosphoSTOP phosphatase inhibitors (Roche). Samples were centrifuged for 10 min at $8,000 \times g$ at 4 °C, and supernatants were removed and stored at −80 °C. Protein concentration was assayed using BCA protein assays (Pierce, Thermo Scientific). For Western blotting, 7.5 μg of protein were loaded into each lane of 4–15% (mg/100 mL) Tris·HCl polyacryamide gels (Bio-Rad). Protein was transferred to Immobilon-P PVDF membranes (Millipore), blocked with 5% (mg/100 mL) BSA (Sigma) for 1 h, and incubated in the following antibody solutions overnight: LIN28A, 1:1,000 (Cell Signaling); α-tubulin, 1:120,000 (Sigma-Aldrich); β-actin, 1:1,200,000 (Abcam). Blots were then incubated in the following horseradish peroxidase-conjugated secondary antibodies for 1 h and 15 min: anti-rabbit IgG, HRP-linked (Cell Signaling), anti-mouse IgG, HRP-linked (Cell Signaling). HRP was subsequently activated and enhanced using SuperSignal West Pico and Femto (Fisher Scientific) chemiluminescent substrate. Bands were visualized using Kodak Biomax MR Film. Blots were then analyzed using ImageJ. For protein measurements of nerve growth factor (NGF) and BDNF, the NGF ELISA kit (Genway) and the BDNF ELISA kit (Genway) were used, respectively, following manufacturer's instructions. For IGF1 protein measurements in the serum, the Mouse/Rat IGF-I Quantikine ELISA Kit was used (R&D Systems).

Behavioral and Autonomic Nervous System Assays. For the rotarod motor coordination assay, an increasing angular-speed rotarod system (Rotarod 7650, Rotamex 4/8; Columbus Instruments) was used in 7-wk-old male and 6- to 12-mo-old female mice. On the first day of testing, the mice were first acclimated to the testing apparatus with three 90-s trials of steadily increasing speed (4–8 rpm). Following this acclimation (first experimental day), three trials of 5 min with increasing speed (4–20 rpm) were conducted. These trials are repeated the following day (second experimental day) without an acclimation period. The latency to fall for each trial was recorded (with a maximum of 300 s), and the three trials were averaged for both the first and second experimental days.

For the three-chamber sociability and social novelty test, both sociability and social memory were tested using a custom-made apparatus with three chambers, for which mice showed no pre-existing chamber preference. Each experimental mouse was acclimated to the three-chamber apparatus for one 5-min trial the 2 d before testing and once directly before testing (3 d total). Before testing (third day), clear plastic tubes were placed in the left and right (#3) chambers and the stimulus mouse was given a 5-min acclimation within a tube. During the test itself, the stimulus mouse was placed within the chamber #1 tube and the experimental mouse was placed in the center chamber #2 and allowed to explore for a 10-min "social approach" (SA) trial. Thirty minutes following this test, each experimental mouse was given another 5-min trial, referred to as the "social recognition" (SR) trial. The percentage of time spent in the chamber holding the stimulus mouse was determined from the video recordings of both the SA and SR trials and was used for further analysis. A minimum number of chamber crossings was used to exclude trials where mice are not physically able to effectively move between chambers.

Vital signs (breath rate and heart rate) were measured in 4- and 8-wk-old animals using an infrared neck sensor (MouseOx; Starr Life Sciences). Fur from the neck was removed 1 d before the test. Animals were acclimated to a test neck clip for 2 h before recording. An infrared neck clip was attached and the mouse's movements were restricted inside a Falcon tube for clearer signal. Vitals measured until at least 4 min of good signal were obtained.

For the open-field test, mice were placed in an empty arena for 15 min. Analysis of percentage of time spent in the center and in the surround was calculated using ImageJ software. MATLAB was used to calculate the total distance traveled by each mouse.

For the locomotion test, an infrared beam device (Pheno-Master-Activity XY; TSE Systems) was used to measure the locomotor activity of mice inside their cages overnight (7:00 PM to 7:00 AM). The first hour was used for animal acclimation and the beam crossings per minute were measured during the remaining 11 h for each animal.

For the objet recognition test, $MeCP2^{+/-}$ mice were placed in an empty arena for 6 min after which four objects of similar size yet different shape were added inside. The mice were left to explore the objects for three more sessions of 6 min each (sessions 2, 3, and 4). At the fifth and last session, two objects were switched diagonally and the mice were let for 6 more minutes into the area. Between each session, mice were transferred

to their cages for 3 min and the objects and the arena were cleaned. A performance ratio was calculated as the ratio of the contacts with the displaced vs. the nondisplaced objects during the last trial divided by the ratio of the contacts with the objects to be switched vs. the objects that were to remain at the same place during the fourth trial when the mice were acclimated to the presence of the original objects.

For respiratory function in unrestrained *Mecp2* heterozygous females, whole-body flow plethysmograph breathing was recorded (EMKA Technologies) during which a constant bias flow supply connected to the animal recording chamber ensured continuous inflow of fresh air (0.8 L/min). Mice were habituated in the plethysmograph chamber to reduce any stress before measurements. For each female, apnea count and inspiratory and expiratory frequency were measured during 12-min periods, once before treatment began and then again after 3 wk of treatment. As apneas, we characterized the absence of respiration for 500 ms. In every measurement, the mice were left for 5 min in the chamber before data recording was initiated.

Statistics. For assessing normal distribution of data, the Kolmogorov–Smirnov test was used. For analysis between sample groups, analysis of variance (ANOVA) with Newman–Keuls multiple-comparison test was applied (WTv vs. KOv and KOt vs. KOv) or in the case of lack of normal data distribution, the Kruskal–Wallis test was used. Pearson correlation was used for all association analysis. The Gehan–Breslow–Wilcoxon test, which allows the presence of censored observations, was chosen for analysis of survival, because a small subset of primarily treated mice included in the graph were euthanized prematurely for tissue extraction or were still alive at the time that the manuscript was written. For comparing overall weight differences between multiple weight values at different ages of the four experimental groups, two-way ANOVA was used and the effects of age and experimental group were separately calculated by unweighted means analysis. For analyzing the difference between behavioral data in female *Mecp2* Het mice before and after treatment with clenbuterol, a two-tailed paired *t* test was used for data with normal distribution and Wilcoxon matched-pairs signed rank test was applied for nonparametric comparisons. Because of the high variability in behavioral performance observed in female *Mecp2* mice, Grubb's extreme Studentized deviate test was applied to all data. No more than one mouse per dataset was excluded for being a significant outlier ($P < 0.05$).
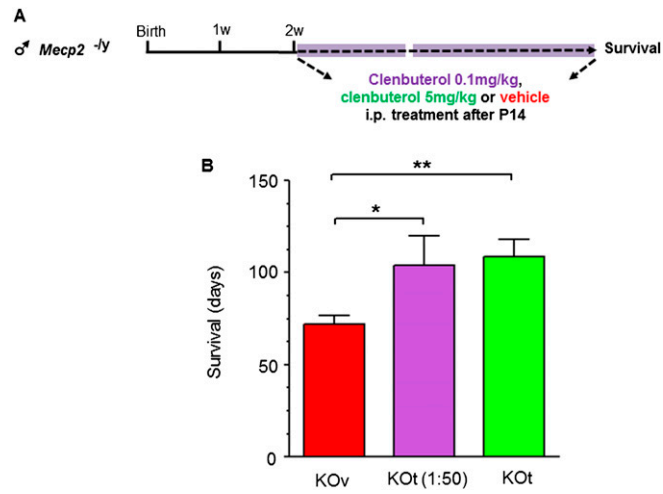
Fig. S1. Lower-dose clenbuterol is equally effective in increasing survival of *Mecp2* KO mice. (*A*) Schematic of treatment duration and dose. (*B*) Graph showing mean ± SEM survival (in days) of KO vehicle (KOv, red bars), KO clenbuterol-treated (KOt, green bars), and 50 times lower dose clenbuterol-treated KO mice [KOt (1:50), green bars]. *n* = 17 for KOv mice, *n* = 13 for KOt, and *n* = 6 for KOt (1:50) mice. The asterisks depict statistical significance based on two-tailed two-sample *t* test (**$P < 0.01$, *$P < 0.05$).
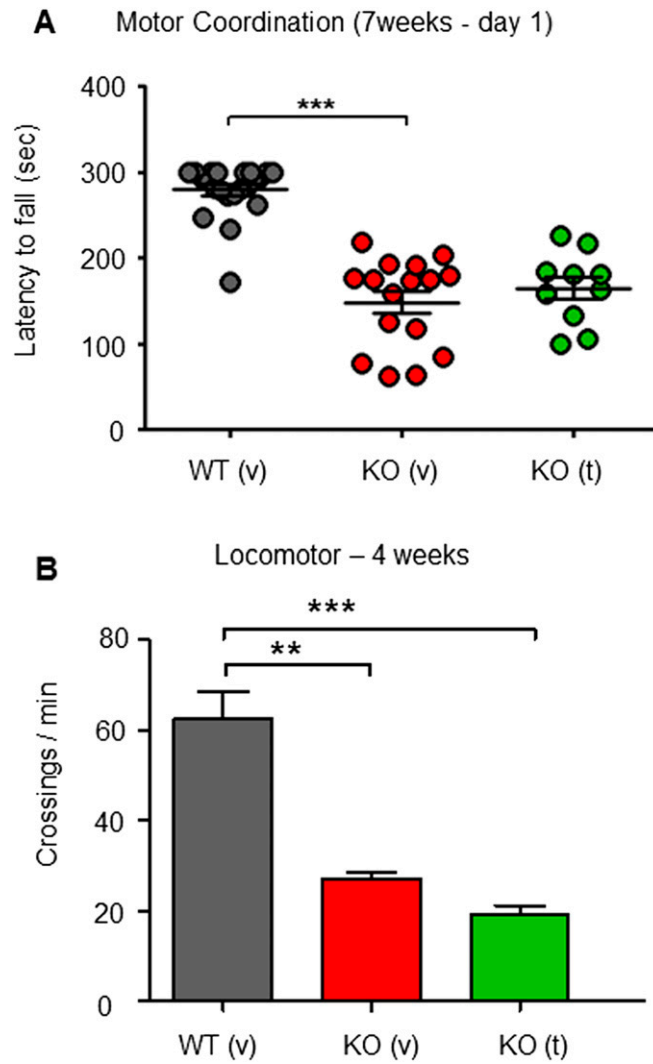
Fig. S2. Clenbuterol effects on the first day of the rotarod motor coordination assay, and locomotion. (*A*) Graph showing mean ± SEM latency to fall rotarod motor coordination test values (in seconds) for the first test day for 7-wk-old WT vehicle [WT (v), black circles], KO vehicle [KO (v), red circles], and clenbuterol-treated [KO (t), green circles] mice. (*B*) Graph showing mean ± SEM crossings per millisecond in 4-wk-old WT vehicle [WT (v), black circles; *n* = 21], KO vehicle [KO (v), red circles; *n* = 5], and clenbuterol-treated [KO (t), green circles; *n* = 12] mice. In both *A* and *B*, the stars depict statistical significance based on ANOVA with Newman–Keuls (***P < 0.001, **P < 0.01).
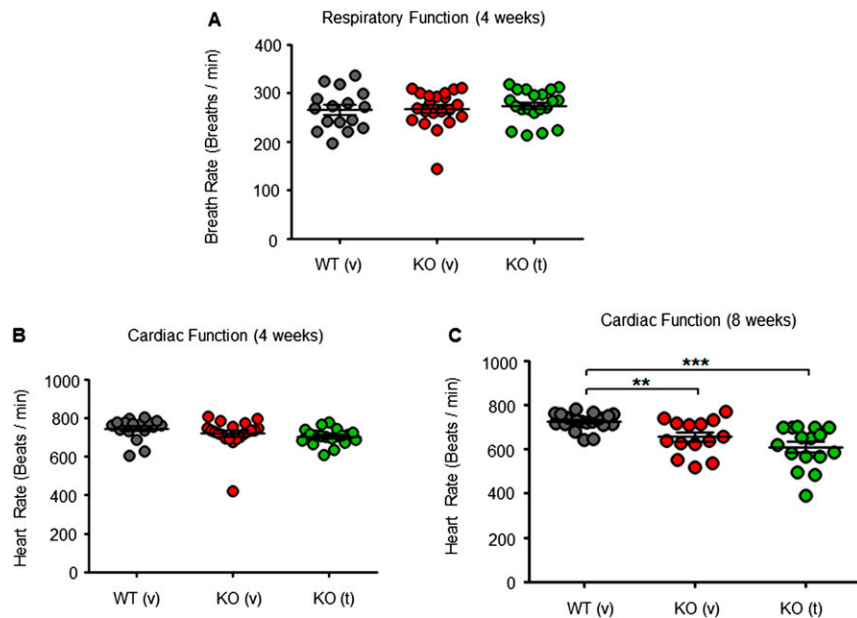
Fig. S3. Effects of clenbuterol on early respiratory function, and heart rate. (*A*) Graph showing mean ± SEM breath rate values (breaths per minute) in 4-wk-old WT vehicle [WT (v), black circles], KO vehicle [KO (v), red circles], and clenbuterol-treated [KO (t), green circles] mice. (*B* and *C*) Graph showing mean ± SEM heart rate values (beats per minute) in both (*B*) 4-wk-old and (*C*) 8-wk-old mice for the same three experimental groups. In all graphs, the stars depict statistical significance based on ANOVA with Newman–Keuls test (***P < 0.001, **P < 0.01, comparing WTv vs. KOv and KOt vs. KOv).
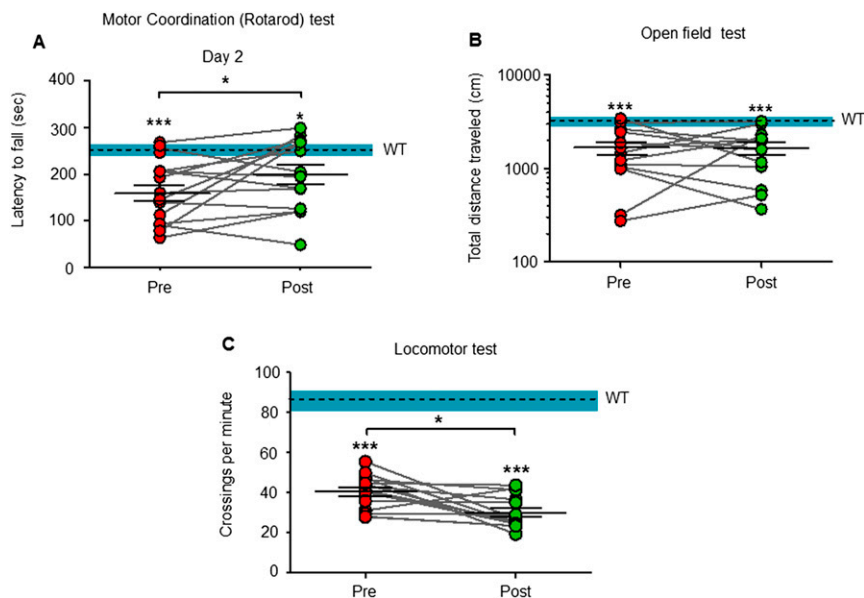
Fig. S4. Influence of clenbuterol on additional behavioral tests in female adult symptomatic *Mecp2*−/+ mice. (*A*) Graph showing latency to fall rotarod motor coordination test values (in seconds) before (filled red circles) and after (filled green circles) 4 wk of clenbuterol treatment. Results from the second experimental day are shown. (*B*) Graph showing the total distance traveled (in centimeters) during the acclimation period before the open-field test. (*C*) Graph showing mean ± SEM crossings per millisecond during the general locomotion assay before and after clenbuterol treatment. The stars between pretreatment and posttreatment in all graphs depict statistical significance based on two-tailed, paired Student *t* test (*P < 0.05), and the stars over data points depict significance relative to WT female mice based on two-tailed, one-sample Student *t* test (***P < 0.001). In all graphs, the dotted line depicts the mean ± SEM values of the female WT control mice.

Fig. S5. Multiple let-7 family miRNAs are increased in *Mecp2* KO mice. (*A*) Graph showing mean ± SEM relative to WT(v) ratios of cerebellar mature let-7a,b,c,d,e,g miRNA levels in KO vehicle [KO (v), red bars; *n* = 5] mice based on mature miRNA qRT-PCR and normalized to snoRNA202. The asterisks depict statistical significance based on one-sample *t* test (**P < 0.01, *P < 0.05). (*B*) Graph showing mean ± SEM cerebellar pri-miR-let-7f-1 and pri-miR-let-7f-2 levels in WT vehicle [WT (v), black bars; *n* = 7], KO vehicle [KO (v), red bars; *n* = 5], and clenbuterol-treated [KO (t), green bars; *n* = 5] mice, based on qRT-PCR and normalized to the geometric mean of 18S rRNA and β-actin.

Fig. S6. Clenbuterol increases NGF levels in the cerebellum of male *Mecp2* null mice. (*A* and *B*) Graph showing mean ± SEM cerebellar NGF mRNA levels based on qRT-PCR and normalized to the geometric mean of 18S rRNA and β-actin (*A*), and NGF protein levels based on ELISA (*B*). Number of samples for WT (v), KO (v), and KO (t) were 7, 5, and 5, respectively, for mRNA, and 11, 8, and 10 for protein levels. In all graphs, the stars depict statistical significance based on ANOVA with Newman–Keuls test for multiple comparisons (**$P < 0.01$, comparing WTv vs. KOv and KOt vs. KOv).

Fig. S7. In vitro LIN28A and let-7f inhibition in Hep G2 cell line. Graph showing mean ± SEM relative to negative controls let-7f (*Left*) and LIN28A mRNA (*Right*) levels in Hep G2 cell line after inhibition of let-7f (let-7f anti-miR; $n = 5$) and shRNA-mediated knockdown of LIN28A (LIN28A shRNA; $n = 5$). Scrambled negative controls for miRNA inhibition (NC anti-miR) and LIN28A shRNA (NC shRNA) were used. The stars depict statistical significance (**$P < 0.01$, *$P < 0.05$) based on two-tailed Student *t* test.
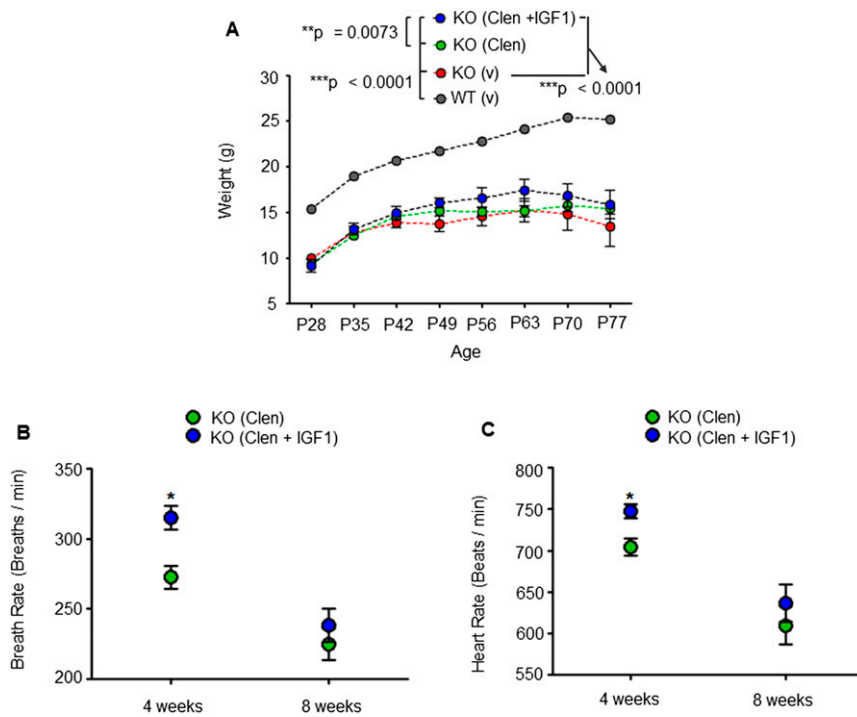
Fig. S8. Weight and cardiorespiratory frequency improvements following cotreatment with clenbuterol and rhIGF1. (*A*) Graph showing means ± SEM of animal weight (in grams) during different ages for *Mecp2* KO mice receiving clenbuterol and rhIGF1 cotreatment [KO (Clen + IGF1), blue circles], as well as WT vehicle-treated mice [WT (v), gray circles]. *P* values shown are based on two-way ANOVA (*Materials and Methods*). (*B*) Graph showing mean ± SEM breath rate values (breaths per minute) for 4- and 8-wk-old clenbuterol-alone [KO (Clen), shown as green circles] and clenbuterol-plus-rhIGF1–treated [KO (Clen + IGF1), shown as blue circles] mice. (*C*) Graph showing mean ± SEM heart rate values (beats per minute) for 4- and 8-wk-old KO (Clen) and KO (Clen + IGF1) mice. In both graphs, the stars represent statistical significance based on two-tailed Mann–Whitney test (*P* < 0.05).